J. Fluid Mech. (1995), *vol.* 296, *pp.* 325–351

The interaction of a moving fluid/fluid interface with a flat plate

By J. BILLINGHAM[1] AND A. C. KING[2]

[1]Schlumberger Cambridge Research, High Cross, Madingley Road, Cambridge CB3 0EL, UK

[2]School of Mathematics and Statistics, University of Birmingham, Edgbaston, Birmingham B15 2TT, UK

(Received 21 December 1994 and in revised form 24 February 1995)

A well-known technique for metering a multiphase flow is to use small probes that utilize some measurement principle to detect the presence of different phases surrounding their tips. In almost all cases of relevance to the oil industry, the flow around such local probes is inviscid and driven by surface tension, with negligible gravitational effects. In order to study the features of the flow around a local probe when it meets a droplet, we analyse a model problem: the interaction of an infinite, initially straight, interface between two inviscid fluids, advected in an initially uniform flow towards a semi-infinite thin flat plate oriented at 90° to the interface. This has enabled us to gain some insight into the factors that control the motion of a contact line over a solid surface, for a range of physical parameter values.

The potential flows in the two fluids are coupled nonlinearly at the interface, where surface tension is balanced by a pressure difference. In addition, a dynamic contact angle boundary condition is imposed at the three-phase contact line, which moves along the plate. In order to determine how the interface deforms in such a flow, we consider the small- and large-time asymptotic limits of the solution. The small-time and linearized large-time problems are solved analytically, using Mellin transforms, whilst the general large-time problem is solved numerically, using a boundary integral method.

The form of the dynamic contact angle as a function of contact line velocity is the most important factor in determining how an interface deforms as it meets and moves over the plate. Depending on this, the three-phase contact line may, at one extreme, hang up on the leading edge of the plate or, at the other extreme, move rapidly along the surface of the plate. At large times, the solution asymptotes to an interface configuration where the contact line moves at the far-field velocity.

1. Introduction

One well-known class of techniques used to meter multiphase flows is based on the use of local probes. These probes must be small (typically hundreds of microns in diameter), so that they disturb the flow as little as possible, and use some measurement principle that distinguishes between the flowing phases. A time series can then be averaged to produce a measurement of the time-averaged, local phase fraction. Two common measurement principles are:

(i) Electromagnetic interaction with the flow. For example laser light can be shone down an optical fibre and the intensity of the reflected light measured (see Sekoguchi

et al. 1985). This technique makes use of the different refractive indices of the flowing fluids.

(ii) Thermal interaction with the flow. For example a small wire can be heated by an electrical current, and its electrical resistivity, which varies with temperature, measured (see Serizawa, Kataoka & Michiyoshi 1974). This is known as a hot-film probe, and makes use of the different thermal properties of the flowing fluids.

Ideally, local probes would be used to measure the local velocity of the flow, as well as the local phase fraction. For the optical probes described by Sekoguchi *et al.* (1985), this was achieved by using the Doppler effect as a moving fluid/fluid interface approaches the probe. Hot-film probes can also be used, since the rate of cooling of the wire increases with fluid velocity (see King 1914). In addition, a time of flight measurement can be made if two local probes, using almost any measurement principle, are located so that a fluid/fluid interface meets one before the other (see Moujaes 1990). From this an interfacial velocity can be deduced.

In order to deduce the global, time-averaged phase fractions and the individual phase flow rates, a number of local measurements must be made across the pipe or annulus in which the multiphase mixture is flowing. These can then be integrated across the flow to yield the required global quantities. The signals from any local probe must be interpretable, accurate, and robust. We therefore need to know what happens when a fluid/fluid interface interacts with a solid local probe, and how this depends on the properties of the fluids and the surface of the probe. This is the vital theoretical background that underpins the interpretation of any local probe measurement, and is the subject of the present paper.

We begin in §2 by examining the size of the four forces (inertia, gravity, viscosity, surface tension) that act when an interface moves past a local probe. We conclude that inertia and surface tension forces usually dominate, and move on, in §3, to study a model inviscid irrotational flow: the advection of an interface past a semi-infinite flat plate. We study the large- and small-time solutions of this model problem, using both asymptotic and numerical methods, in §4 and §5, and make some observations about the possible behaviour of the solution for all times in §6. We consider how the model problem can be related indirectly to the deformation of an interface interacting with a local probe in §7, and conclude in §8.

2. Typical dimensions, fluid properties and dimensionless groups

The important oilfield activity known as production logging involves lowering a string of various tools into a producing oil well and measuring flow rates and phase fractions in a flow of oil and water. Typical values for fluid density, ρ, density difference, $\Delta\rho$, fluid viscosity, μ, surface tension, σ, fluid velocity, v, and probe diameter, d, are given in table 1. The lower value for the surface tension given in table 1 is smaller than values often quoted in the literature, but our measurements have shown that this is a good estimate for crude oil and saline water.

The four forces that act when an oil/water interface passes a local probe are inertia, gravity, viscosity and surface tension. We can estimate the relative magnitude of these forces by calculating the Reynolds, capillary, Weber, Froude and Bond numbers (*Re*, *Ca*, *We*, *Fr* and *Bo*). These dimensionless groups are defined in table 2, where ranges of possible values are also shown.

We find that, in general, $Re \gg 1$, $Ca \ll 1$, $Fr \gg 1$, $Bo \ll 1$, whilst the Weber number, *We*, can be moderately small or large, with size mainly dependent on the value of the fluid velocity. From this we conclude that viscosity and gravity are

Liquid density	ρ	$800 - 1000\ \mathrm{kg\,m^{-3}}$
Density difference	$\Delta\rho$	$0 - 200\ \mathrm{kg\,m^{-3}}$
Liquid viscosity	μ	$10^{-3}\ \mathrm{kg\,m^{-1}s^{-1}}$
Surface tension	σ	$0.05 - 0.005\ \mathrm{N\,m^{-1}}$
Velocity	v	$0.1 - 2\ \mathrm{m\,s^{-1}}$
Probe diameter	d	$200\ \mu\mathrm{m} - 1.2\ \mathrm{mm}$

TABLE 1. Typical dimensions and fluid properties for production logging.

Re	$\rho v d/\mu$	16 – 2400
Ca	$\mu v/\sigma$	0.002 – 0.4
We	$\rho v^2 d/\sigma$	0.032 – 960
Fr	$\rho v^2/\Delta\rho g d$	3.3 – ∞
Bo	$\Delta\rho g d^2/\sigma$	0 – 0.6

TABLE 2. Typical values of dimensionless groups for production logging.

generally negligible compared to inertia and surface tension. Of course, viscosity will always act in the boundary layer on the surface of the probe, but we shall not consider the effect of this here.

To illustrate how these dimensionless groups appear in the governing equations and boundary conditions, consider the typical dimensionless momentum equation

$$\frac{\partial \bar{\boldsymbol{u}}_A}{\partial \bar{t}} + \bar{\boldsymbol{u}}_A \cdot \bar{\nabla}\bar{\boldsymbol{u}}_A = -\bar{\nabla}\bar{p}_A^* + Re^{-1}\bar{\nabla}^2\bar{\boldsymbol{u}}_A + Fr^{-1}\boldsymbol{k}, \tag{2.1}$$

and the typical normal stress interfacial boundary condition

$$\frac{1}{\bar{R}} = [-We\,\bar{p} + Ca\,\boldsymbol{n}\cdot\bar{\boldsymbol{e}}\cdot\boldsymbol{n}]_B^A + Bo\,\bar{z}, \tag{2.2}$$

where an overbar indicates a dimensionless variable, $p^* \equiv p - \rho_B g z$ is the reduced pressure, z measures distance in the direction of gravity and the subscripts A and B indicate the fluid properties on either side of an interface. Velocity, length, time and pressure have been made dimensionless using v, d, d/v and ρv^2 respectively. The dimensionless radius of curvature of the interface is $\bar{R}$, the unit normal to the interface is $\boldsymbol{n}$, the unit vector in the direction of gravity is $\boldsymbol{k}$, the dimensionless normal viscous stress is $\boldsymbol{n}\cdot\bar{\boldsymbol{e}}\cdot\boldsymbol{n}$, and the square brackets indicate the difference across the interface. For the sizes of dimensionless groups discussed above, we can see that (2.1) reduces to the Euler momentum equation, with momentum flux balanced by the pressure gradient ($Re \gg 1$, $Fr \gg 1$), whilst the normal stress boundary condition (2.2) has surface tension forces balanced by the pressure difference across the interface ($Ca \ll 1$, $Bo \ll 1$). Note that the size of the Weber number, *We*, determines the size of the pressure difference needed to sustain a given curvature.

3. A model problem

When a local probe penetrates an interface, two processes are crucial in determining the shape of the interface. Firstly, as the interface becomes close to the probe a thin film forms between the interface and the point of closest approach. For example, when an interface approaches a sharp-tipped local probe a thin film forms over the tip. The rate at which fluid drains from this film determines how long it takes for the

Secondly, once the interface meets the surface of the probe, a three-phase contact line is formed and the interface moves to form the thermodynamically determined contact angle that is appropriate to the two fluids, the solid surface, and also the speed at which the contact line is able to move across the surface of the probe, consistent with the outer flow.

The approach that we have adopted is to try to study each of these processes separately and in detail, using simplified model problems. The main simplifications used have been in the geometry of the solid surface and the symmetry of the interfacial deformation. We are currently studying the process of film drainage at the point of contact with the probe by analysing the motion of a fluid/fluid interface past a fixed solid sphere. This will not be examined here.

The subject of the present paper is the motion of the interface once it has made contact with the surface of the probe. The model problem that we have studied is a fluid/fluid interface moving past a thin, semi-infinite, flat plate. Since the plate is thin, the interface is simply advected to meet the leading edge of the plate, so that the film drainage process is eliminated. The problem is two-dimensional, and we shall assume that the flow velocity is uniform before the interface meets the plate. Also, on the basis of our analysis of the relative importance of the various forces given in §2, we shall neglect gravity and assume that the flow is inviscid and incompressible. Note that we are *not* suggesting that this model problem is part of an asymptotic solution for the flow around a local probe, valid close to the contact line (although this may be possible in some cases). Our objectives are, for the moment, less ambitious. We are interested in relating the qualitative form of the solution of the model problem to the behaviour of interfaces on a length scale appropriate to local probes, and in determining how this varies with the size of the probe, the fluid properties and the far-field velocity, as discussed in §7.

3.1. *Governing equations*

The two-dimensional coordinate system (x, y) is illustrated in figure 1, along with the configuration of the plate and fluid/fluid interface. The plate is initially surrounded by fluid B, which is displaced by fluid A. The position of the interface is given by $y = Y(x,t)$, where t is time. When $t < 0$, the interface and all of the fluid translates uniformly in the y-direction at velocity u_∞, so that $Y(x,t) = u_\infty t$. At $t = 0$ the interface touches the leading edge of the plate and a contact line is formed. When $t > 0$, this contact line at $y = y_c(t)$ moves along the plate at velocity $u_c(t)$, where u_c may be zero. In addition, the contact angle, θ_c, as defined in figure 1(*c*), is a known function of u_c. The system is symmetric about the line $x = 0$, which includes the plate, and we shall confine our attention to the domain $x \geqslant 0$. A mathematical statement of the problem is made easier if we define two domains of fluid flow,

$$D_A = \{(x,y) : 0 \leqslant x < \infty, -\infty < y \leqslant Y(x,t)\}, \tag{3.1a}$$

$$D_B = \{(x,y) : 0 \leqslant x < \infty, Y(x,t) \leqslant y < \infty\}, \tag{3.1b}$$

so that D_A contains the fluid A and D_B the fluid B.

Since the fluids are inviscid and the flow is initially irrotational, the flow remains irrotational. We can therefore define velocity potentials, ϕ_A and ϕ_B, in D_A and D_B respectively as

$$\boldsymbol{u}_A = \nabla\phi_A, \quad \boldsymbol{u}_B = \nabla\phi_B, \tag{3.2}$$

where $\boldsymbol{u}_A$ and $\boldsymbol{u}_B$ are the velocity fields in D_A and D_B. Each potential then satisfies

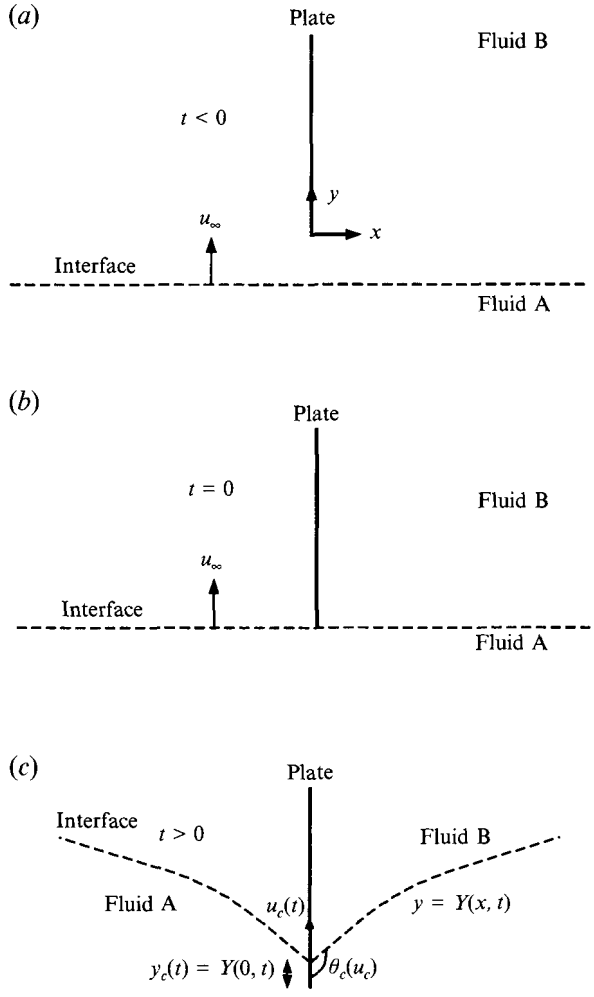

FIGURE 1. The configuration of the plate and interface when (*a*) $t < 0$, (*b*) $t = 0$, (*c*) $t > 0$.

Laplace's equation,

$$\nabla^2\phi_A = 0 \text{ in } D_A, \quad \nabla^2\phi_B = 0 \text{ in } D_B. \tag{3.3}$$

The symmetry condition at $x = 0$ is (where ϕ_A and ϕ_B are understood to be defined only in D_A and D_B respectively)

$$\phi_{A,x} = 0, \quad \phi_{B,x} = 0, \quad \text{on } x = 0. \tag{3.4}$$

On the interface itself we have continuity of normal velocity,

$$\phi_{A,y} - \phi_{A,x}Y_x = \phi_{B,y} - \phi_{B,x}Y_x, \tag{3.5}$$

the interface advection equation,

$$\phi_{A,y} = Y_t + \phi_{A,x}Y_x, \tag{3.6}$$

and continuity of normal stress,

$$\tfrac{1}{2}(\rho_A - \rho_B)u_\infty^2 + \tfrac{1}{2}\rho_B|\nabla\phi_B|^2 + \rho_B\phi_{B,t} - \tfrac{1}{2}\rho_A|\nabla\phi_A|^2 - \rho_A\phi_{A,t} = -\sigma Y_{xx}/(1+Y_x^2)^{3/2}, \tag{3.7}$$

all for $y = Y(x,t)$. Here $\rho_{A,B}$ are the densities of the two fluids and σ is the surface

tension. In addition to these equations we impose uniform flow conditions at infinity so that

$$\phi_{A,B} \to u_\infty y, \quad Y \to u_\infty t, \quad \text{as } x \to \infty. \tag{3.8}$$

Finally the contact angle condition that must be specified on the plate is

$$Y_x(0,t) = -\cot\theta_c(u_c), \tag{3.9}$$

where the velocity of the contact line is

$$u_c(t) = \phi_{A,y}(0, Y(0,t)). \tag{3.10}$$

This completes the definition of the boundary value problem.

In order to obtain more tractable boundary conditions at infinity, we define

$$\phi_{A,B} = u_\infty y + \phi^*_{A,B}, \quad y^* = y - u_\infty t, \quad Y^* = Y - u_\infty t. \tag{3.11}$$

By subtracting from the original variables the uniform flow behaviour at infinity, (3.8) become

$$\phi^*_{A,B} \to 0, \quad Y^* \to 0, \quad \text{as } x \to \infty. \tag{3.12}$$

In terms of the starred variables, (3.3) to (3.6) and (3.9) remain the same, but (3.7) becomes

$$\tfrac{1}{2}\rho_B |\nabla\phi^*_B|^2 + \rho_B \phi^*_{B,t} - \tfrac{1}{2}\rho_A |\nabla\phi^*_A|^2 - \rho_A \phi^*_{A,t} = -\sigma Y^*_{xx}/(1 + Y^{*2}_x)^{3/2}. \tag{3.13}$$

The problem is now formulated in a frame of reference where the fluid is initially stationary and the plate is moving.

3.2. *Dimensionless variables*

The only fluid properties that appear in the problem are density, ρ, and surface tension, σ. We also have the uniform flow velocity, u_∞. From these, the only quantity that we can form with dimensions of length is $\sigma/\rho u_\infty^2$. We can think of this as the length scale on which surface tension balances inertia. In contrast to the dimensionless variables used in (2.1) and (2.2), there is no geometrical length scale in this problem, so we define

$$\bar{x} = x \Big/ \frac{\sigma}{\rho_A u_\infty^2}, \quad \bar{y} = y^* \Big/ \frac{\sigma}{\rho_A u_\infty^2}, \quad \bar{Y} = Y^* \Big/ \frac{\sigma}{\rho_A u_\infty^2}, \tag{3.14 a–c}$$

$$\bar{\phi}_{A,B} = \phi^*_{A,B} \Big/ \frac{\sigma}{\rho_A u_\infty}, \quad \bar{t} = t \Big/ \frac{\sigma}{\rho_A u_\infty^3}. \tag{3.14 d,e}$$

Note that we have arbitrarily chosen to use the density of fluid A in these definitions. In terms of the new variables, (3.14), the boundary value problem becomes

$$\nabla^2\bar{\phi}_A = 0 \ \text{ in } D_A, \quad \nabla^2\bar{\phi}_B = 0 \ \text{ in } D_B, \tag{3.15}$$

subject to

$$\bar{\phi}_{A,\bar{x}} = 0, \quad \bar{\phi}_{B,\bar{x}} = 0, \quad \text{on } \bar{x} = 0, \tag{3.16}$$

$$\bar{\phi}_{A,\bar{y}} - \bar{\phi}_{A,\bar{x}}\bar{Y}_{\bar{x}} = \bar{\phi}_{B,\bar{y}} - \bar{\phi}_{B,\bar{x}}\bar{Y}_{\bar{x}}, \tag{3.17}$$

$$\bar{\phi}_{A,\bar{y}} = \bar{Y}_{\bar{t}} + \bar{\phi}_{A,\bar{x}}\bar{Y}_{\bar{x}}, \tag{3.18}$$

$$\rho\left(\tfrac{1}{2}|\nabla\bar{\phi}_B|^2 + \bar{\phi}_{B,\bar{t}}\right) - \tfrac{1}{2}|\nabla\bar{\phi}_A|^2 - \bar{\phi}_{A,\bar{t}} = -\bar{Y}_{\bar{x}\bar{x}}/(1 + \bar{Y}^2_{\bar{x}})^{3/2}, \tag{3.19}$$

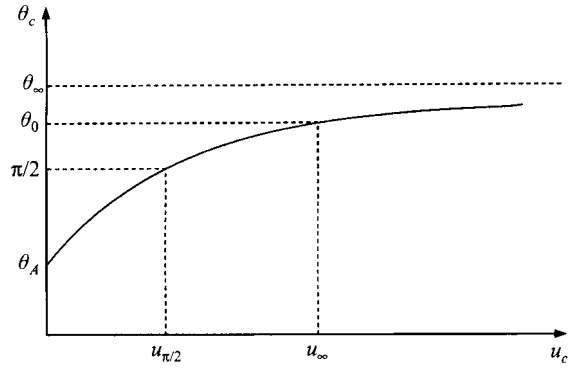

FIGURE 2. The dynamic contact angle for positive contact line velocities.

with (3.17) to (3.19) applied at the interface, $\bar{y} = \bar{Y}(\bar{x}, \bar{t})$, and

$$\bar{\phi}_{A,B} \to 0, \quad \bar{Y} \to 0, \quad \text{as } \bar{x} \to \infty, \tag{3.20}$$

$$\bar{Y}_{\bar{x}}(0, \bar{t}) = -\cot\theta_c. \tag{3.21}$$

In these equations, the ratio of the fluid densities is $\rho = \rho_B/\rho_A$.

3.3. *The dynamic contact angle*

In order to proceed, we need to make some assumptions about how the dynamic contact angle, θ_c, varies with contact line speed, u_c. Clearly, the exact functional form of θ_c depends on the two fluids and the nature of the solid surface. However, there are some generic features that θ_c is known to possess (see Dussan V. 1979). Firstly, static contact angle hysteresis is almost always observed. This means that there is a range of possible static contact angles, $\theta_R \leqslant \theta_c(0) \leqslant \theta_A$, where θ_R is known as the receding contact angle, and θ_A the advancing contact angle. Secondly, except for certain polymeric fluids, θ_c is monotonic. In the context of this report we shall find that we are only interested in positive contact line velocities. We shall therefore assume that θ_c is qualitatively of the form shown in figure 2. We also find it useful to define θ_∞ to be the limiting value of θ_c as $u_c \to \infty$, and $u_{\pi/2}$ to be the contact line velocity at which $\theta_c = \pi/2$. Note that if $\theta_\infty < \pi/2$ or $\theta_A > \pi/2$, $u_{\pi/2}$ does not exist. Finally, we define θ_0 to be the dynamic contact angle when the contact line velocity is u_∞, the uniform flow velocity.

Now that we have defined the boundary value problem, our task is to determine how the fluid/fluid interface, described by $\bar{Y}(\bar{x}, \bar{t})$, deforms for various values of the static advancing contact angle, θ_A, the limiting, large-velocity contact angle, θ_∞, and the density ratio, ρ. There is no analytical solution of this problem, and a numerical solution would not be easy to obtain. However, we can use asymptotic methods to analyse the large- and small-time solutions of the problem. These give us a good idea of the qualitative behaviour of the interface for all $\bar{t} > 0$, which we shall describe in §6. We shall also show, in §7, that these solutions can be directly related to the cases of large and small Weber number when we consider the deformation of an interface on a length scale appropriate for a local probe.

4. Large-time solution

The boundary value problem defined by (3.15) to (3.21) contains no length or velocity scale. If the contact angle were independent of contact line velocity, this would mean that there must be a self-similar solution, valid for all $\bar{t} > 0$. However, as $\bar{t} \to \infty$ we expect that θ_c tends to some constant value, and hence that this similarity solution will be the large-time limit of the solution to the boundary value problem. It is straightforward to show that the appropriate similarity variables are

$$\xi = \frac{\bar{x}}{\bar{t}^{2/3}}, \quad \eta = \frac{\bar{y}}{\bar{t}^{2/3}}, \quad \Phi(\xi,\eta) = \frac{\bar{\phi}}{\bar{t}^{1/3}}, \quad \hat{y}(\xi) = \frac{\bar{Y}}{\bar{t}^{2/3}}. \tag{4.1}$$

In terms of these similarity variables, the dimensionless velocity of the moving contact line is $\bar{u}_c = 1 - (2/3)\,\bar{t}^{-1/3}\hat{y}(0)$. Therefore, as $\bar{t} \to \infty$, $\bar{u}_c \to 1$. In terms of the physical variables, this means that the contact line velocity approaches the uniform flow velocity, u_∞, as $t \to \infty$. As a consequence, $\theta_c \to \theta_0$ as $t \to \infty$. Of course, this argument presupposes that $\hat{y}(0)$ is bounded for all values of θ_0. This will be investigated below.

In terms of the similarity variables (4.1), the boundary value problem becomes

$$\nabla^2 \Phi_A = 0 \ \text{ in } D_A, \quad \nabla^2 \Phi_B = 0 \ \text{ in } D_B, \tag{4.2}$$

subject to

$$\Phi_{A,\xi} = 0, \quad \Phi_{B,\xi} = 0, \quad \text{on } \xi = 0, \tag{4.3}$$

$$\Phi_{A,\eta} - \Phi_{A,\xi}\hat{y}_\xi = \Phi_{B,\eta} - \Phi_{B,\xi}\hat{y}_\xi, \tag{4.4}$$

$$\Phi_{A,\eta} = \tfrac{2}{3}\left(\hat{y} - \xi\hat{y}_\xi\right) + \Phi_{A,\xi}\hat{y}_\xi, \tag{4.5}$$

$$\rho\left\{\tfrac{1}{2}|\nabla\Phi_B|^2 + \tfrac{1}{3}\Phi_B - \tfrac{2}{3}\left(\xi\Phi_{B,\xi} + \hat{y}\Phi_{B,\eta}\right)\right\}$$

$$-\tfrac{1}{2}|\nabla\Phi_A|^2 - \tfrac{1}{3}\Phi_A + \tfrac{2}{3}\left(\xi\Phi_{A,\xi} + \hat{y}\Phi_{A,\eta}\right) = -\hat{y}_{\xi\xi}/\left(1+\hat{y}_\xi^2\right)^{3/2}, \tag{4.6}$$

with (4.4) to (4.6) applied at the interface, $\eta = \hat{y}(\xi)$, and

$$\Phi_{A,B} \to 0, \quad \hat{y} \to 0, \quad \text{as } \xi \to \infty, \tag{4.7}$$

$$\hat{y}_\xi(0) = -\cot\theta_0. \tag{4.8}$$

A numerical solution of this free boundary problem was calculated for the case $\rho = 0$, by Keller & Miksis (1983), and an asymptotic study was carried out by King (1991). Before we solve this boundary value problem numerically, it is instructive to consider a linearized solution of the problem, valid when the contact angle, θ_0, is close to $\pi/2$. This solution can be used to check the accuracy of the numerical solution of the full nonlinear problem, and gives us some insight into the dynamics of the interface.

4.1. *The linearized problem*

Consider the case where there is near orthogonal contact between the interface and the plate. We let $\theta_0 = \pi/2 + \epsilon$, with $\epsilon \ll 1$, and pose asymptotic expansions in the form

$$\hat{y} = \epsilon\tilde{y} + o(\epsilon),$$

$$\Phi_{A,B} = \epsilon\tilde{\Phi}_{A,B} + o(\epsilon). \tag{4.9}$$

The leading-order linearized form of the boundary value problem is

$$\nabla^2\tilde{\Phi}_A = 0 \ \text{ in } D_A, \quad \nabla^2\tilde{\Phi}_B = 0 \ \text{ in } D_B, \tag{4.10}$$

subject to

$$\tilde{\Phi}_{A,\xi} = 0, \quad \tilde{\Phi}_{B,\xi} = 0, \quad \text{on } \xi = 0. \tag{4.11}$$

At leading order, the domains D_A and D_B are the quarter-planes $0 \leqslant \xi < \infty$, $-\infty < \eta \leqslant 0$ and $0 \leqslant \xi < \infty$, $0 \leqslant \eta < \infty$ respectively. The interface conditions, which are to be applied on $\eta = 0$ for $0 < \xi < \infty$, are

$$\tilde{\Phi}_{A,\eta} = \tilde{\Phi}_{B,\eta}, \tag{4.12}$$

$$\tilde{\Phi}_{A,\eta} = \tfrac{2}{3}\left(\tilde{y} - \xi \tilde{y}_\xi\right), \tag{4.13}$$

$$\rho\left\{\tfrac{1}{3}\tilde{\Phi}_B - \tfrac{2}{3}\xi\tilde{\Phi}_{B,\xi}\right\} - \tfrac{1}{3}\tilde{\Phi}_A + \tfrac{2}{3}\xi\tilde{\Phi}_{A,\xi} = -\tilde{y}_{\xi\xi}, \tag{4.14}$$

and

$$\tilde{\Phi}_{A,B} \to 0, \quad \tilde{y} \to 0, \quad \text{as } \xi \to \infty, \tag{4.15}$$

$$\tilde{y}_\xi(0) = 1. \tag{4.16}$$

We note that both $\tilde{\Phi}_A$ and $\tilde{\Phi}_B$ satisfy Laplace's equation, have no normal derivative on $\xi = 0$, and (4.12) shows that they have equal normal derivatives on $\eta = 0$. This shows that $\tilde{\Phi}_A(\xi,\eta) = -\tilde{\Phi}_B(\xi,-\eta)$. We therefore define $\tilde{\Phi} \equiv \tilde{\Phi}_B$, and find that $\tilde{\Phi}$ satisfies

$$\nabla^2\tilde{\Phi} = 0 \quad \text{for } 0 \leqslant \xi < \infty, \ -\infty < \eta \leqslant 0, \tag{4.17}$$

subject to

$$\tilde{\Phi}_\xi = 0, \quad \text{on } \xi = 0, \tag{4.18}$$

$$\tilde{\Phi}_\eta = \tfrac{2}{3}\left(\tilde{y} - \xi\tilde{y}_\xi\right), \quad \text{on } \eta = 0, \tag{4.19}$$

$$(1+\rho)\left\{\tfrac{1}{3}\tilde{\Phi} - \tfrac{2}{3}\xi\tilde{\Phi}_\xi\right\} = -\tilde{y}_{\xi\xi}, \quad \text{on } \eta = 0, \tag{4.20}$$

and

$$\tilde{\Phi} \to 0, \quad \tilde{y} \to 0, \quad \text{as } \xi \to \infty, \tag{4.21}$$

$$\tilde{y}_\xi(0) = 1. \tag{4.22}$$

This boundary value problem can be solved using Mellin integral transforms. We shall show in §5 that a very similar boundary value problem can govern the leading-order behaviour of the small-time asymptotic solution. In order to derive a general solution that we can use for both of these problems, we rewrite the boundary value problem given by (4.17) to (4.22) in terms of polar coordinates (r,θ), a potential Φ and an interface position y, as

$$\nabla^2\Phi = 0 \quad \text{for } 0 \leqslant r < \infty, \ 0 \leqslant \theta \leqslant \pi/2, \tag{4.23}$$

subject to

$$\Phi_\theta = 0, \quad \text{on } \theta = 0, \tag{4.24}$$

$$\Phi_\theta = \tfrac{2}{3}r\left(ry_r - k_0 y\right), \quad \text{on } \theta = \pi/2, \tag{4.25}$$

$$\tfrac{1}{3}(1+\rho)\left\{k_1\Phi - k_2 r\Phi_r\right\} = -y_{rr}, \quad \text{on } \theta = \pi/2, \tag{4.26}$$

$$\Phi \to 0, \quad y \to 0, \quad \text{as } r \to \infty, \tag{4.27}$$

and

$$y_r(0) = 1. \tag{4.28}$$

For the case that we are interested in here, $k_0 = 1$, $k_1 = 1$ and $k_2 = 2$. We can solve the general boundary value problem given by (4.23) to (4.28) using Mellin integral

transforms, but first we must establish the behaviour of the solution close to and far from the contact line at $r = 0$.

4.2. *Solution for* $r \ll 1$

For $r \ll 1$ we pose coordinate expansions in the form

$$\Phi = A + rB(\theta) + O(r^2), \quad y = a_0 + a_1 r + a_2 r^2 + O(r^3). \tag{4.29}$$

By substituting these expansions into (4.23) to (4.26) we find that $B = \frac{2}{3}k_0 a_0 \cos\theta$ and $A = -6a_2/k_1(1+\rho)$. Hence all of the differential equations and boundary conditions can be satisfied by the above expansions, and we would expect this asymptotic structure to emerge from the integral transform solution.

4.3. *Solution for* $r \gg 1$

For $r \gg 1$ we pose coordinate expansions of the form

$$\Phi = \frac{C\cos\theta}{r} + \ldots + \frac{D\cos 4\theta}{r^4} + \ldots, \quad y = \frac{E}{r^2} + \ldots . \tag{4.30}$$

Laplace's equation (4.23) is clearly satisfied by these multipole solutions, along with (4.24). On substituting these expansions into (4.25) and (4.26) we find that $C = \frac{2}{3}(k_0 + 2)E$ and $D = -18E/(k_1 + 4k_2)(1+\rho)$. Again we conclude that all of the differential equations and boundary conditions can be satisfied by the above expansions. We therefore expect this asymptotic structure to appear in the integral transform solution. It is worth noting that an oscillatory term may appear in the above expansions but that it is not dominant.

4.4. *The integral transform solution*

We define the Mellin transforms of the potential and interface as

$$\Phi^*(p,\theta) = \int_0^\infty r^{p-1}\Phi(r,\theta)\,\mathrm{d}r, \tag{4.31a}$$

$$y^*(p) = \int_0^\infty r^{p-1} y(r)\,\mathrm{d}r. \tag{4.31b}$$

These transforms generally exist, and are analytic functions in some strip of the complex p-plane. The behaviour of Φ and y for small and large r shows that the transform of Φ is analytic in $0 < \mathrm{Re}(p) < 1$, whilst the transform of y is analytic in $0 < \mathrm{Re}(p) < 2$. The transformed version of Laplace's equation in each region is a simple ordinary differential equation with solution that satisfies (4.24),

$$\Phi^* = B(p)\cos p\theta. \tag{4.32}$$

The kinematic condition (4.25) leads to

$$(p-1)B(p-1)\sin\{\pi(p-1)/2\} = \tfrac{2}{3}(k_0 + p)y^*(p). \tag{4.33}$$

A Mellin transform of (4.26) gives the relationship

$$\tfrac{1}{3}(1+\rho)(k_1 + k_2 p)B(p) = -(p-1)(p-2)y(p-2). \tag{4.34}$$

Some simple algebraic manipulation shows that a single equation for B can be found in the form

$$\frac{B(p)}{B(p-3)} = -\frac{9}{2(1+\rho)}\frac{(p-1)(p-2)(p-3)}{(p-2+k_0)(k_1+k_2 p)}. \tag{4.35}$$

The solution to this functional difference equation is

$$B(p) = \left\{\frac{27}{2|k_2|(1+\rho)}\right\}^{p/3} \frac{\Gamma\left(\frac{1}{3}p+\frac{2}{3}\right)\Gamma\left(\frac{1}{3}p+\frac{1}{3}\right)\Gamma\left(\frac{1}{3}p\right)}{\Gamma\left(\frac{1}{3}p+\frac{1}{3}(k_0+1)\right)\Gamma\left(\frac{1}{3}p+(k_1+3k_2)/3k_2\right)} b(p), \quad (4.36)$$

where

$$\begin{aligned} b(p) &= -b(p-3), \quad \text{for } k_2 > 0, \\ b(p) &= b(p-3), \quad \text{for } k_2 < 0. \end{aligned} \quad (4.37)$$

With the structure of $B(p)$ known we can work backwards and find that

$$\Phi^* = -\left\{\frac{27}{2|k_2|(1+\rho)}\right\}^{p/3} \frac{\Gamma\left(\frac{1}{3}p+\frac{2}{3}\right)\Gamma\left(\frac{1}{3}p+\frac{1}{3}\right)\Gamma\left(\frac{1}{3}p\right)\cos(p\theta)\, b(p)}{\Gamma\left(\frac{1}{3}p+\frac{1}{3}(k_0+1)\right)\Gamma\left(\frac{1}{3}p+(3k_2+k_1)/3k_2\right)}, \quad (4.38)$$

$$y^* = -\frac{3}{2}\left\{\frac{27}{2|k_2|(1+\rho)}\right\}^{p/3-1/3} \frac{(p-1)}{(p+k_0)} \frac{\Gamma\left(\frac{1}{3}p+\frac{1}{3}\right)\Gamma\left(\frac{1}{3}p\right)\Gamma\left(\frac{1}{3}p-\frac{1}{3}\right)\cos\left(\frac{1}{2}p\pi\right) b(p-1)}{\Gamma\left(\frac{1}{3}p+\frac{1}{3}k_0\right)\Gamma\left(\frac{1}{3}p+(2k_2+k_1)/3k_2\right)}. \quad (4.39)$$

It now remains to choose $b(p)$ so that the transforms are analytic in the appropriate strip of the p-plane and also have the correct behaviour as $r \to 0$ and $r \to \infty$. We firstly note that as $|p| \to \infty$ (with $p = p_1 + ip_2$), y^* and Φ^* are of $O\left(b(p)\, e^{\pm \pi p_2/3}/p^{\alpha}\right)$ as $p_2 \to \pm\infty$, with p_1 fixed, where α is a positive constant. In order to ensure convergence of the transform integrals we need $b(p)$ to decay at least as fast as $e^{\mp \pi p_2/3}$.

If we consider the singularity structure of the transforms in the half-plane $\mathrm{Re}(p) \leqslant 0$, with $k_0 = 1$, $k_1 = 1$ and $k_2 = 2$, neglecting for the moment any singularities in $b(p)$, we see that

$$\left.\begin{aligned} &y^* \text{ has simple poles at } p = 0, -2, -3, \ldots, \text{ but no pole at } p = -1, \\ &\Phi^* \text{ has simple poles at } p = 0, -1, -3, \ldots, \text{ but no pole at } p = -2. \end{aligned}\right\} \quad (4.40)$$

To obtain the correct structure for y as $r \to 0$, y^* must have a simple pole at $p = -1$. Hence $b(p)$ must have a simple pole at $p = -2$. Notice that this forces $b(p)$ to have another simple pole at $p = 1$. However, the resulting poles at $p = 1$ in the expression for Φ^* and $p = 2$ in the expression for y^* are allowable, since Φ^* is analytic only in $0 < \mathrm{Re}(p) < 1$ and y^* only in $0 < \mathrm{Re}(p) < 2$. It is now apparent from (4.37) that $b(p)$ is an anti-periodic function, with period 3, and also that $b(p)$ has a simple pole at $p = -2$ and exponential decay at infinity. Therefore, $b(p)$ is of the form

$$b(p) = \frac{\beta(p)}{\sin\left(\frac{1}{3}\pi(p+2)\right)}, \quad (4.41)$$

where $\beta(p)$ is a strictly periodic function satisfying $\beta(p) = \beta(p-3)$. Since y^* is analytic in $0 < \mathrm{Re}(p) < 2$, $\beta(p-1)$ must also be analytic there. If $\beta(p-1)$ had a pole in $-1 < \mathrm{Re}(p) \leqslant 0$, say at $p = -\mu$ with $0 < \mu < 1$, then we would find that

$$y \sim y(0) + ar^{\mu} + r, \quad \text{as } r \to 0. \quad (4.42)$$

The presence of the r^{μ} term in this expansion violates the contact angle and curvature conditions at the origin. This shows that $\beta(p)$ must be analytic in $-1 < \mathrm{Re}(p) < 2$, and therefore, from its periodicity, analytic in the whole of the complex p-plane. It must also be bounded for large $|p|$ if the transform integrals are to converge. Hence, by Liouville's Theorem, it is a constant, and we write $\beta(p) = \beta$.

In order to find the value of β we need to apply (4.28). If we close the inversion contour of the Mellin inversion integral by a large semi-circle lying in $-\infty < \mathrm{Re}(p) < 0$,

a process that is valid due to the decay of the inverse transform on the semi-circle, we find that

$$y(r) = \frac{1}{2\pi i}\int_{c-i\infty}^{c+i\infty} y^*(p)\, r^{-p} dp = \Sigma_{p\leqslant 0} \text{ Residues at poles of } y^*(p)\, r^{-p}, \tag{4.43}$$

where c is a real constant with $0 < c < 2$. A simple residue calculation at the poles $p = 0, -1$ shows that

$$y(r) = -\frac{3}{2}\left(\frac{27}{4(1+\rho)}\right)^{-1/3} \times \beta\left\{\frac{-2\Gamma\left(-\frac{1}{3}\right)}{\sqrt{3}\Gamma\left(\frac{5}{6}\right)} - \left(\frac{27}{4(1+\rho)}\right)^{-1/3}\frac{3\Gamma\left(-\frac{2}{3}\right)\Gamma\left(-\frac{1}{3}\right)r}{\Gamma\left(\frac{1}{2}\right)} + O\left(r^2\right)\right\}, \tag{4.44}$$

for $r \ll 1$. Applying $y_r(0) = 1$ gives $\beta = \frac{2}{9}\{27/4(1+\rho)\}^{2/3}\Gamma\left(\frac{1}{2}\right)/\Gamma\left(-\frac{2}{3}\right)\Gamma\left(-\frac{1}{3}\right)$ and hence $y(0) = \frac{2}{9}\sqrt{3}\{27/4(1+\rho)\}^{1/3}\Gamma\left(\frac{1}{2}\right)/\Gamma\left(-\frac{2}{3}\right)\Gamma\left(\frac{5}{6}\right)$. If the gamma functions are replaced by their numerical values we find that

$$y(0) = -0.852(1+\rho)^{-1/3}. \tag{4.45}$$

Now, using the original variables, the solution for $\tilde{y}$ is given by

$$\tilde{y}(\xi) = -\frac{2}{27}\left(\frac{27}{4(1+\rho)}\right)^{1/3}\frac{\Gamma\left(\frac{1}{2}\right)}{\Gamma\left(\frac{1}{3}\right)\Gamma\left(\frac{2}{3}\right)}\frac{1}{2\pi i}$$

$$\int_{c-i\infty}^{c+i\infty}\left(\frac{27}{4(1+\rho)}\right)^{p/3}\frac{\Gamma\left(\frac{1}{3}p-\frac{1}{3}\right)\Gamma\left(\frac{1}{3}p\right)(p-1)\cos(\frac{1}{2}\pi p)\xi^{-p}}{\Gamma\left(\frac{1}{3}p+\frac{5}{6}\right)(1+p)\sin(\frac{1}{3}\pi(p+1))}dp, \tag{4.46}$$

with $0 < c < 2$. Although this form is closed, there is no simple expression for it in terms of elementary functions, and the interfacial deformation must be computed from (4.46). This was done numerically using a composite trapezium rule, evaluating the gamma functions using the routine given in Press *et al.* (1986). Graphs of $\tilde{y}$ as a function of ξ, for $\rho = 0.05$, 0.8, 1.2 and 20 are illustrated in figure 3. A typical density ratio for oil and water is $\rho = 0.8$ or 1.2. The ratios $\rho = 0.05$ and 20 have been included to show the effect of a greater density contrast. We note that the form of the solution for $\rho = \rho_1 > 1$ is simply a scaled version of the solution for $\rho = 1/\rho_1 < 1$, with the scaling given by

$$\tilde{y}(\xi;\rho) \equiv \rho^{-1/3}\tilde{y}\left(\rho^{-1/3}\xi;\rho^{-1}\right), \quad \text{for all } \rho \geqslant 0. \tag{4.47}$$

Figure 3 shows that a decaying capillary wave propagates along the interface. In the Appendix, we show that the wavelength decays as ξ^{-2} and the amplitude as $\xi^{-7/2}$, as $\xi \to \infty$, and determine the asymptotic behaviour of $\tilde{y}$ in this limit. Remember that ξ and $\tilde{y}$ are scaled variables, and must each be multiplied by $(\theta_0 - \pi/2)\,\bar{t}^{2/3}$ to recover the unscaled dimensionless variables. In terms of the dimensionless variables, although the amplitude of the wave decays as $\bar{x} \to \infty$, the amplitude grows as $\bar{t}$ increases at any fixed point $\bar{x} \gg 1$. The plate exerts a point force on the fluid at the contact line in order to maintain the required contact angle. This force generates waves that propagate away from the force with an amplitude that decays, even though there is no dissipative mechanism present (see, for example, Jeffreys & Jeffreys 1962).

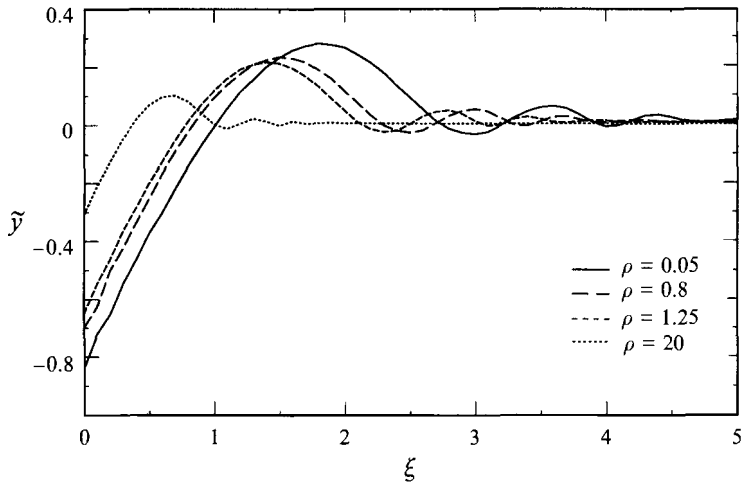

FIGURE 3. Graphs of the solution (4.46) for various values of ρ.

In terms of the original physical variables, the position of the moving contact line is given by

$$y_c(t) \sim u_\infty t - 0.852\left(\theta_0 - \frac{\pi}{2}\right)\left(\frac{\sigma}{\rho_A + \rho_B}\right)^{1/3} t^{2/3}, \quad \text{as } t \to \infty. \tag{4.48}$$

If $\theta_0 > \pi/2$ the contact line lags behind the far-field interface, and *vice versa*. Note that if $\theta_0 = \pi/2$, the interface remains undeformed and normal to the plate, since this simple solution satisfies the contact angle condition (4.16).

4.5. *The full nonlinear problem*

As we noted earlier, if the contact angle, θ_0, is not close to $\pi/2$, we must resort to numerical methods to solve the boundary value problem given by (4.2) to (4.8). We have developed an efficient numerical solution method for the boundary value problem given by (4.2) to (4.8), based on Green's integral representation for harmonic functions.

In two dimensions, the harmonic function, Φ_A, satisfies

$$\pi\Phi_A(\boldsymbol{r}_0) \equiv \int_{\partial D_A} \left\{ \Phi_A(\boldsymbol{r}) \frac{\partial}{\partial n_A} \ln|\boldsymbol{r} - \boldsymbol{r}_0| - \frac{\partial \Phi_A}{\partial n_A}(\boldsymbol{r}) \ln|\boldsymbol{r} - \boldsymbol{r}_0| \right\} \mathrm{d}s, \tag{4.49}$$

where ∂D_A is the boundary of the domain, D_A, in which Φ_A is harmonic, $\boldsymbol{n}_A$ is the outward unit normal, $\boldsymbol{r}$, $\boldsymbol{r}_0 \in \partial D_A$, and $\mathrm{d}s$ is an element of arc length. The equivalent equation holds for Φ_B. For fluid A, the outward unit normal to the domain D_A is

$$\boldsymbol{n} = (-\hat{y}(\xi), 1)/(1 + \{\hat{y}'(\xi)\}^2)^{1/2}. \tag{4.50}$$

The outward unit normal to the domain D_B, occupied by the fluid B, has the opposite sign. We can eliminate $\partial\Phi_A/\partial n$ from (4.49) by using the kinematic condition (4.5) in the form

$$\frac{\partial \Phi_A}{\partial n} = \tfrac{2}{3}\{\xi\hat{y}'(\xi) - \hat{y}(\xi)\}/(1 + \{\hat{y}'(\xi)\}^2)^{1/2}. \tag{4.51}$$

Using the integral representation given by (4.49) we can now formulate the problem in terms of the values of the potentials Φ_A and Φ_B on the interface alone, which we

shall denote by

$$\psi_{A,B}(\xi) \equiv \Phi_{A,B}(\xi, \hat{y}(\xi)). \tag{4.52}$$

After some simple algebraic manipulation exploiting the symmetry of the flow across $\xi = 0$, we can rewrite (4.49) as

$$\begin{aligned}\pi\psi_A(\xi_0) = \int_0^\infty \psi_A(\xi) \Bigg[& \frac{(\xi-\xi_0)\hat{y}'(\xi) + \hat{y}(\xi_0) - \hat{y}(\xi)}{(\xi-\xi_0)^2 + \{\hat{y}(\xi) - \hat{y}(\xi_0)\}^2} \\ & + \frac{(\xi+\xi_0)\hat{y}'(\xi) + \hat{y}(\xi_0) - \hat{y}(\xi)}{(\xi+\xi_0)^2 + \{\hat{y}(\xi) - \hat{y}(\xi_0)\}^2} \Bigg] \mathrm{d}\xi \\ & + \frac{1}{3}\int_0^\infty \{\xi\hat{y}'(\xi) - \hat{y}(\xi)\} \Big[\ln\Big[(\xi-\xi_0)^2 + \{\hat{y}(\xi) - \hat{y}(\xi_0)\}^2\Big] \\ & + \ln\Big[(\xi+\xi_0)^2 + \{\hat{y}(\xi) - \hat{y}(\xi_0)\}^2\Big]\Big] d\xi. \end{aligned} \tag{4.53}$$

A similar equation holds for ψ_B, with changes of sign to account for the direction of the outward normal to the region D_B.

We must now rewrite (4.6) in terms of ψ_A and ψ_B, using expressions for $\Phi_{A,B,\xi}$ and $\Phi_{A,B,\eta}$ in terms of derivatives of the potential at the interface. By definition,

$$\psi_A'(\xi) = \Phi_{A,\xi} + \Phi_{A,\eta}\hat{y}'(\xi), \tag{4.54}$$

which, along with (4.5), leads to

$$\Phi_{A,\xi} = \left[\tfrac{2}{3}\hat{y}'(\xi)\{\xi\hat{y}'(\xi) - \hat{y}(\xi)\} + \psi_A'(\xi)\right] / \left[1 + \{\hat{y}'(\xi)\}^2\right], \tag{4.55}$$

and

$$\Phi_{A,\eta} = \left[\hat{y}'(\xi)\psi_A'(\xi) - \tfrac{2}{3}\hat{y}'(\xi)\{\xi\hat{y}'(\xi) - \hat{y}(\xi)\}\right] / \left[1 + \{\hat{y}'(\xi)\}^2\right]. \tag{4.56}$$

Similar expressions can be found for $\Phi_{B,\xi}$ and $\Phi_{B,\eta}$.

We now define a mesh of discrete points $\xi = \xi_i = ih$, for $i = 0, 1, \ldots, n$, with corresponding values of the unknowns, $\psi_A^i \equiv \psi_A(\xi_i)$, $\psi_B^i \equiv \psi_B(\xi_i)$ and $\hat{y}_i \equiv \hat{y}(\xi_i)$. The discretized form of (4.5) is

$$\begin{aligned} & \rho\left[\tfrac{1}{3}\psi_B^i - \tfrac{2}{3}\left(\xi_i\Phi_{B,\xi}^i + \hat{y}_i\Phi_{B,\eta}^i\right) + \tfrac{1}{2}\left\{\left(\Phi_{B,\xi}^i\right)^2 + \left(\Phi_{B,\eta}^i\right)^2\right\}\right] \\ & - \tfrac{1}{3}\psi_A^i + \tfrac{2}{3}\left(\xi_i\Phi_{A,\xi}^i + \hat{y}_i\Phi_{A,\eta}^i\right) - \tfrac{1}{2}\left\{\left(\Phi_{A,\xi}^i\right)^2 + \left(\Phi_{A,\eta}^i\right)^2\right\} = -\hat{y}_i'' / \left\{1 + \left(\hat{y}_i'\right)^2\right\}^{3/2}, \end{aligned} \tag{4.57}$$

for $i = 1, \ldots, n-1$. After substituting (4.55) and (4.56) into (4.57), all derivatives can be approximated by central differences to $O(h^2)$ accuracy. We can discretize the integral equations satisfied by ψ_A and ψ_B (given by (4.53) for ψ_A and a similar equation for ψ_B) by truncating the infinite range at nh and using a composite trapezium rule. This gives $O(h^2)$ accuracy. The equation for ψ_A^i takes the form

$$\pi\psi_A^i = \frac{1}{2}h\sum_{j=0}^{n} w_j\psi_A^j K_{ij} - \frac{1}{6}h\sum_{j=0, j\neq i}^{n} w_j\left(\xi_j\hat{y}_j' - \hat{y}_j\right)L_{ij} - M(h, \hat{y}_i), \tag{4.58}$$

for $i = 1, \ldots, n-1$. In this discretized equation, w_j are the weights appropriate to the trapezium rule,

$$K_{ij} = \frac{\left(\xi_j - \xi_i\right)\hat{y}_j' + \hat{y}_i - \hat{y}_j}{\left(\xi_i - \xi_j\right)^2 + \left(\hat{y}_i - \hat{y}_j\right)^2} + \frac{\left(\xi_j + \xi_i\right)\hat{y}_j' + \hat{y}_i - \hat{y}_j}{\left(\xi_i + \xi_j\right)^2 + \left(\hat{y}_i - \hat{y}_j\right)^2}, \tag{4.59}$$

and

$$L_{ij} = \ln\left\{(\xi_j - \xi_i)^2 + (\hat{y}_j - \hat{y}_i)^2\right\} + \ln\left\{(\xi_j + \xi_i)^2 + (\hat{y}_j - \hat{y}_i)^2\right\}. \tag{4.60}$$

In order to explain why the quantity $M(h, \hat{y}_i)$ appears in (4.58) we note that the integral in (4.53) that involves the quantity $\ln\left[(\xi - \xi_0)^2 + \{\hat{y}(\xi) - \hat{y}(\xi_0)\}^2\right]$ is singular as $\xi \to \xi_0$. By an analytic integration over the range $[\xi_{i-1}, \xi_{i+1}]$, we find that, in order to be consistent with the error in the trapezoidal discretization, we require that

$$M(h, \hat{y}_i) = \tfrac{2}{3}\left(\xi_i \hat{y}_i' - \hat{y}_i\right)\left[2(h \ln h - h) + h \ln\left\{1 + (\hat{y}_i')^2\right\}\right]. \tag{4.61}$$

We now have $3(n-1)$ equations and $3(n+1)$ unknowns. The boundary conditions that close the discretized system are

$$\psi_A^n = \psi_B^n = \hat{y}_n = 0, \tag{4.62}$$

and

$$\hat{y}_0' = -\cot\theta_0, \qquad \psi_{A,B}'(0) = -\tfrac{2}{3}\hat{y}_0 \cot\theta_0. \tag{4.63}$$

The derivatives that arise in (4.63) can be approximated by forward differencing, again accurate to $O(h^2)$. The result of this discretization is a system of $3(n+1)$ nonlinear algebraic equations. These were solved using the NAG routine C05NBF. This uses a combination of steepest descents and Newtonian iterations.

For contact angles close to $\pi/2$, we use an initial estimate of the solution for this iterative scheme with all of the discretized values equal to zero. The resulting solution reproduces the linearized solution derived in §4.1 to within the correct accuracy. For contact angles further from $\pi/2$, this linearized solution can be used as the initial estimate. For contact angles more than about $\pi/4$ from the normal we used a continuation method, with the solution computed for a nearby contact angle used as the initial estimate.

Some typical solutions are shown in figure 4 for $\rho = 0.05$, and in figure 5 for $\rho = 0.8$. As we noted above, the solution for $\rho > 1$ can be obtained using the scaling given by (4.47), in this case for $\hat{y}$. For these numerical solutions we used a grid spacing, h, of 0.05, with 150 grid points, so that the solution was computed for $0 \leqslant \xi \leqslant 7.5$. We were able to obtain solutions unless the contact angle was close to zero or π. The value of ρ made little difference to the range of contact angles for which we could calculate solutions, roughly $0.27 < \theta_0 < 2.87$. The difficulty is that, as the contact angle becomes close to zero or π, so that the interface becomes tangential to the plate, the value of y changes rapidly over a thin region close to the plate. Since the grid is uniform in the ξ-direction, the number of grid points in this region of rapid change becomes insufficient to allow the solution to be approximated accurately. By decreasing the grid spacing we can slightly extend the range of contact angles for which we can compute solutions, but at the expense of a large increase in computing time. The law of diminishing returns seems to operate, and further grid refinement is not a viable method of examining the full range of possible contact angles.

It is clear that a non-uniform grid, with a high concentration of grid points close to the plate is needed to compute solutions with high or low contact angle. Such a grid could be generated adaptively, based on the form of the solution at a nearby contact angle where the solution can be computed. We have not yet pursued this further, since a uniform grid is sufficient to cover the range of contact angles encountered so far during our experiments with local probes.

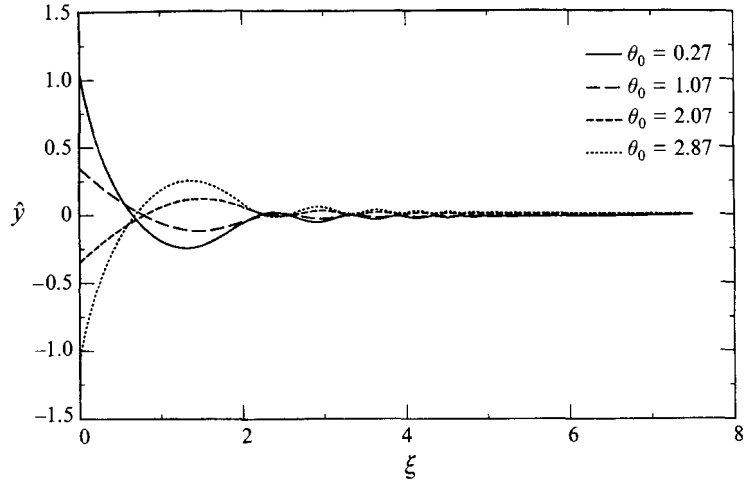

FIGURE 4. Graphs of the interface when $\bar{t} \gg 1$ for various values of θ_0 with $\rho = 0.05$.

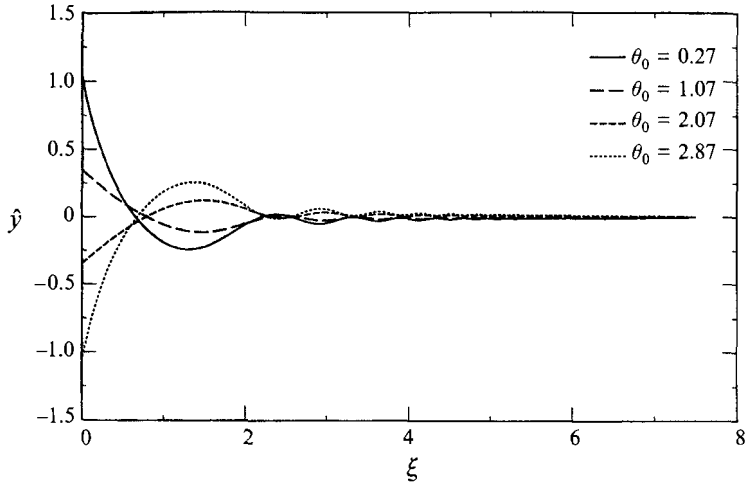

FIGURE 5. Graphs of the interface when $\bar{t} \gg 1$ for various values of θ_0 with $\rho = 0.8$.

Clearly, the contact line lies further from the point $\eta = 0$ the closer θ_0 is to zero or π. As we shall see in §6, we would like to know whether $\hat{y}(0)$ becomes unbounded or tends to a finite limit as $\theta_0 \to 0$ and $\theta_0 \to \pi$. The behaviour of $\hat{y}(0)$ is shown in figure 6. Firstly, we can certainly say that, for fairly small and large contact angles (up to $\theta_0 = 0.27$ or 2.87 radians, equivalently 15° or 165°) $\hat{y}(0)$ is close to unity. Secondly, the trend indicated by figure 6 suggests that $\hat{y}(0)$ remains bounded as $\theta_0 \to 0$ and $\theta_0 \to \pi$.

5. Small-time solution

In the previous section we analysed the natural similarity solution to the boundary value problem defined by (3.15) to (3.21), and found that it represents the long-time limit of the full solution of the problem. It is natural to consider whether this

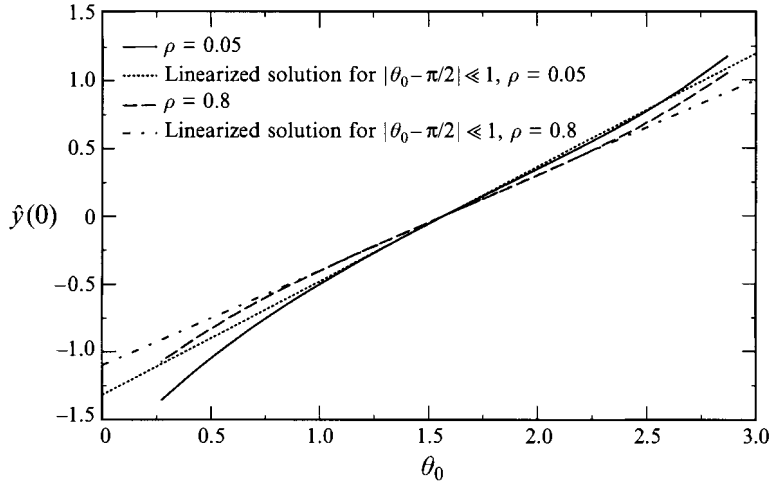

FIGURE 6. Graphs of the position of the contact line for $\bar{t} \gg 1$, for $\rho = 0.05$ and $\rho = 0.8$. The analytical solution of the linearized problem for θ_0 close to $\pi/2$ is also shown in each case.

similarity solution can represent the solution of the boundary value problem at small times, $\bar{t} \ll 1$.

We found above that the velocity of the contact line in the similarity solution is $\bar{u}_c = 1 - (2/3)\,\bar{t}^{-1/3}\hat{y}(0)$. Clearly, if $\bar{t} \ll 1$, the fluid velocity for $\bar{x}$ and $\bar{y}$ of $O(\bar{t}^{2/3})$ is singular, of $O(\bar{t}^{-1/3})$. This suggests that there will be further asymptotic regions for $\bar{t} \ll 1$, where viscosity becomes important. We shall not consider this further here, but simply note that this singularity in the velocity field as $\bar{t} \to 0$ does not prevent the inviscid incompressible similarity solution from being valid at small times. However, we shall see below that the contact angle condition (4.8) means that the similarity solution cannot always represent the small-time solution. There are three cases.

5.1. *Case I:* $\theta_\infty < \pi/2$

As we have seen, the contact line velocity is large at small times in the similarity solution. This means that, if this solution is to be valid, it must satisfy $\hat{y}_\xi(0) = -\cot\theta_\infty$, where θ_∞ is the limiting value of $\theta_c(\bar{u}_c)$ as $\bar{u}_c \to \infty$. If $\theta_\infty < \pi/2$, we have seen in §4 that the contact line has $\bar{y}_c > 0$. This means that, for $\bar{t} \ll 1$, the contact line moves rapidly along the plate, with $\bar{y}_c = O(\bar{t}^{2/3})$, and the similarity solution with $\theta_c = \theta_\infty$ is the leading-order small-time solution.

Note that it is mathematically possible, although physically unlikely, that $\theta_\infty = 0$, and hence that $\theta_c \equiv 0$ for all $\bar{u}_c \geqslant 0$, since we assume that θ_c is monotonic. In this case, the form of the small-time solution is crucially dependent on whether or not $\hat{y}(0) \to \infty$ as $\theta_\infty \to 0$, as discussed in §4.5. If, as seems likely, $\hat{y}(0)$ remains bounded, the small-time position of the contact line is given by

$$\bar{y}_c(\bar{t}) \sim \hat{y}(0; \theta_c = 0)\,\bar{t}^{2/3}. \tag{5.1}$$

However, if this is not the case and $\hat{y}(0) \to \infty$ as $\theta_\infty \to 0$, the contact line must immediately move to infinity at $\bar{t} = 0^+$ and the similarity solution (which now does not include a contact line, since it has moved instantaneously to infinity) is valid for all $\bar{t} > 0$.

If $\theta_\infty > \pi/2$, we have found that $\bar{y}_c < 0$. This is not possible for $\bar{t} \ll 1$, since the contact line cannot leave the plate and retain the characteristics of a contact line.

Clearly, the small-time solution must have some other asymptotic structure in this case.

5.2. *Case II:* $\theta_\infty > \pi/2$, $\theta_A < \pi/2$

By looking for scaled variables that lead to a leading-order balance of terms in (3.15) to (3.21), we find that appropriate definitions are

$$\xi = \frac{\bar{x}}{\bar{t}^{2/3}}, \quad \eta = \frac{\bar{y}}{\bar{t}^{2/3}}, \quad \bar{\Phi}(\xi,\eta) = \frac{\bar{\phi}}{\bar{t}^{2/3}\left(\bar{u}_{\pi/2}-1\right)}, \quad \chi(\xi) = \frac{\left(\bar{Y}/\bar{t}-1\right)}{\left(\bar{u}_{\pi/2}-1\right)}. \tag{5.2}$$

The factors of $\left(\bar{u}_{\pi/2}-1\right)$ above, and the slightly unusual definition of χ are included in order to reduce the boundary conditions to a convenient form, scaling $\bar{u}_{\pi/2}$ out of the leading-order problem, as we shall see below. The coordinates $\bar{x}$ and $\bar{y}$ are scaled with $\bar{t}^{2/3}$, as they were in the similarity scaling (4.1), but now $\bar{\phi}$ also scales with $\bar{t}^{2/3}$, so that the fluid velocity remains of $O(1)$, and the position of the interface, $\bar{Y}$, scales with $\bar{t}$, so that it remains close to both the leading edge of the plate and its far-field position, $\bar{Y} = \bar{t}$. Physically, this means that the velocity of the contact line remains bounded when the interface meets the plate at time $\bar{t} = 0$, since the form of the dynamic contact angle as a function of the contact line velocity allows the contact line initially to remain close to the leading-edge of the plate.

In terms of the scaled variables (5.2), at leading order we obtain a pair of coupled boundary value problem defined on two quarter-planes. Using identical arguments to those given in §4.1 we can reduce this to a single boundary value problem on a quarter-plane in terms of $\bar{\Phi} \equiv \bar{\Phi}_B(\xi,\eta) = -\bar{\Phi}_A(\xi,-\eta)$, given by

$$\nabla^2\bar{\Phi} = 0 \quad \text{for } 0 \leqslant \xi < \infty, \ -\infty < \eta \leqslant 0, \tag{5.3}$$

subject to

$$\bar{\Phi}_\xi = 0, \quad \text{on } \xi = 0, \tag{5.4}$$

$$\bar{\Phi}_\eta = \chi - \tfrac{2}{3}\xi\chi_\xi, \quad \text{on } \eta = 0, \tag{5.5}$$

$$\tfrac{2}{3}(1+\rho)\left\{\bar{\Phi} + \xi\bar{\Phi}_\xi\right\} = -\chi_{\xi\xi}, \quad \text{on } \eta = 0, \tag{5.6}$$

and

$$\bar{\Phi} \to 0, \quad \chi \to 0, \quad \text{as } \xi \to \infty. \tag{5.7}$$

The contact angle boundary condition (3.21) becomes $\bar{y}_{\bar{x}}(0) \ll 1$ as $\bar{t} \to 0$. This means that the contact angle must be $\pi/2$ at leading order. For this to be possible, the contact line must move with velocity $\bar{u}_{\pi/2}$. Taking into account the factors of $\left(\bar{u}_{\pi/2}-1\right)$ in the definition (5.2) of χ, this means that the contact angle boundary condition is equivalent to

$$\chi(0) = 1. \tag{5.8}$$

Before we study the boundary value problem (5.3) to (5.8) we consider the last of the three cases.

5.3. *Case III:* $\theta_\infty > \pi/2$, $\theta_A > \pi/2$

In this case, the only contact line velocity that allows that contact angle to be $\pi/2$ at leading order, and also keeps the contact line on the plate is $\bar{u}_c = 0$. In other words the contact line hangs up on the leading edge of the plate. The appropriate leading-order boundary value problem that we must solve is again given by (5.3) to (5.8), but with $\bar{u}_{\pi/2} = 0$ in the definitions (5.2) of the scaled variables. The behaviour of the dynamic contact angle in each of the three different cases is illustrated in figure 7.

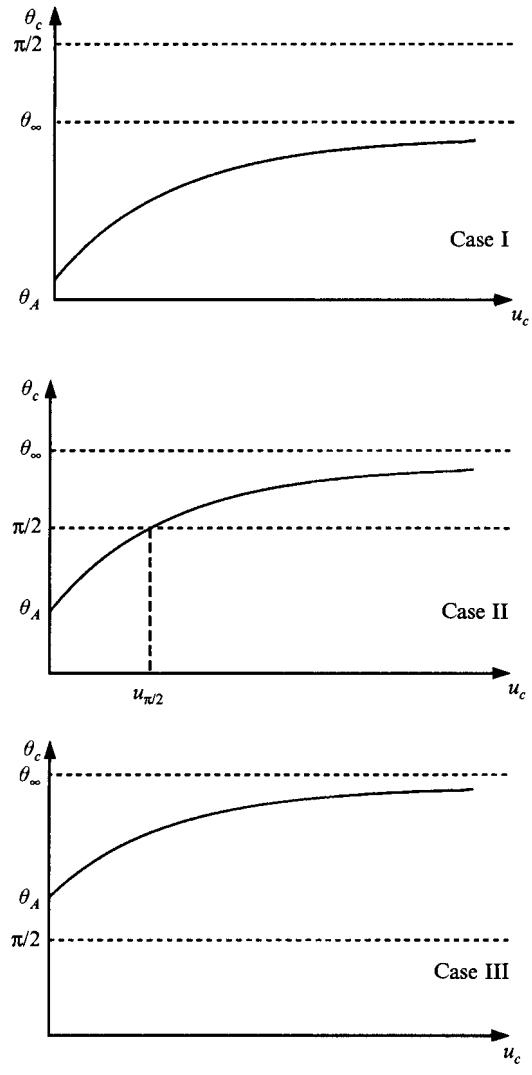

FIGURE 7. The qualitative form of the dynamic contact angle in the three different cases that determine the form of the small-time solution.

It now remains to solve the linear boundary value problem given by (5.3) to (5.8). This has the same form as the boundary value problem (4.23) to (4.27), but with $k_0 = 3/2$, $k_1 = 2$ and $k_2 = -2$, and the boundary condition at the contact line

$$y(0) = 1. \tag{5.9}$$

For this case, the singularity structure of the transforms is as given by (4.40), and similar arguments show that y^* must have a simple pole at $p = -1$. However, in this case, neglecting the singularities of $b(p)$ for the moment, y^* has a zero at $p = -1$. This shows that $b(p)$ must have a *double* pole at $p = -2$. A suitable function is

$$b(p) = \frac{\beta(p)}{\sin^2(\frac{1}{3}\pi(p+2))}, \tag{5.10}$$

since (4.37) shows that $b(p)$ must be strictly periodic in this case. The same arguments

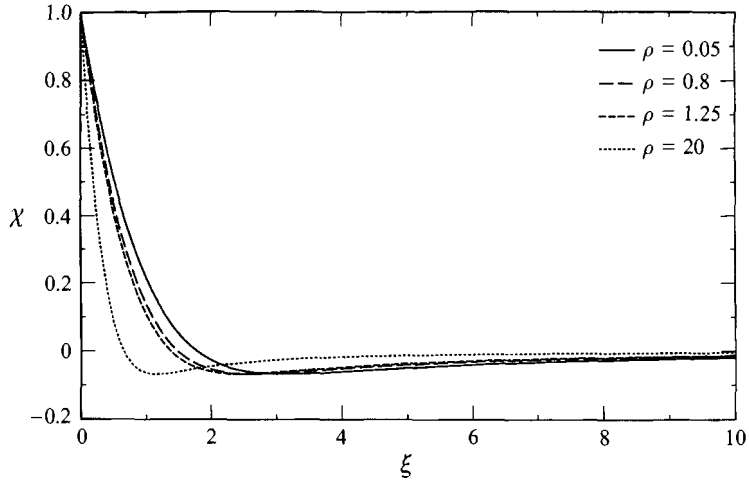

FIGURE 8. Graphs of the solution (5.11) for various values of ρ.

as those given above show that $\beta(p)$ must be constant. Applying the contact line condition (5.9), $y(0) = 1$, shows that $\beta = -\{\frac{1}{12}\pi^{1/2}\Gamma(\frac{2}{3})\}\{27/2(1+\rho)\}^{1/3}$, and hence, using the original variables, that

$$\chi(\xi) = -\frac{\mathrm{i}}{16\pi^{1/2}\Gamma(\frac{2}{3})}\int_{c-\mathrm{i}\infty}^{c+\mathrm{i}\infty}\left(\frac{27}{2(1+\rho)}\right)^{p/3}\frac{\Gamma(\frac{1}{3}p+\frac{2}{3})\,\Gamma(\frac{1}{3}p)\cos(\frac{1}{2}\pi p)\xi^{-p}}{\Gamma(\frac{1}{3}p+\frac{3}{2})\sin^2(\frac{1}{3}\pi(p+1))}\mathrm{d}p, \quad (5.11)$$

with $0 < c < 2$. Although this form is closed, no simple expression for it in terms of elementary functions can be found and the interfacial deformation must be computed numerically from (5.11). This was done by using a composite trapezium rule, evaluating the gamma functions using the routine given in Press *et al.* (1986). Graphs of χ as a function of ξ, for $\rho = 0.05$, 0.8, 1.25 and 20, are shown in figure 8. These solutions should be compared to those shown in figure 3, which are valid both for $\bar{t} \gg 1$ and, in case I, for $\bar{t} \ll 1$. The small-time solutions shown in figure 8 are not oscillatory, and have just a single turning point. In case I, the large impulsive change in velocity at $\bar{t} = 0$ leads to the immediate formation of capillary waves. However, in cases II and III, the capillary waves that have developed when $\bar{t} \gg 1$ must be formed later, when $\bar{t} = O(1)$.

6. The qualitative behaviour of the solution for $\bar{t} > 0$

We are now in a position to speculate about the form of the solution of the initial/boundary value problem defined by (3.15) to (3.21) by considering the form of the small- and large-time solutions derived above. We must consider the three cases, defined in §5, that lead to qualitatively different behaviour at small times.

6.1. *Case I:* $\theta_\infty < \pi/2$

In this case, for $\bar{t} \ll 1$ the solution takes the form of the similarity solution governed by (4.2) to (4.8), and illustrated in figures 4 and 5, but with contact angle θ_∞, the limit of θ_c as $\bar{u}_c \to \infty$. We shall not consider the physically unrealistic case, $\theta_\infty \equiv 0$. For $\bar{t} \gg 1$, the solution also takes the form of this similarity solution, but with $\theta_c = \theta_0 < \theta_\infty$. Figure 9 shows the likely qualitative form of the solution for $\theta_0 = 0.47$

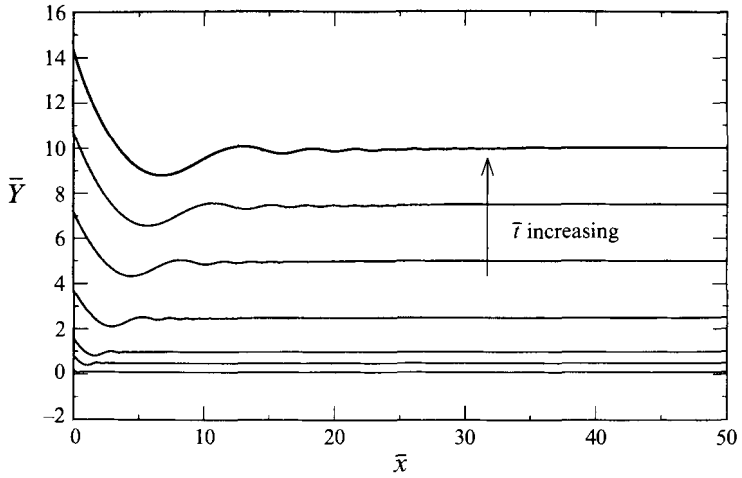

FIGURE 9. Graphs of the qualitative form of the solution for $\theta_0 = 0.47$ and $\theta_\infty = 1.07$ at various times, $\bar{t} = 0.1, 0.5, 1, 2.5, 5, 7.5, 10$. The contact angle decreases by 0.1 radians on each curve. (Case I.)

and $\theta_\infty = 1.07$. This has been constructed by taking the numerically calculated solutions illustrated in figure 4, scaling them appropriately with $\bar{t}$, assuming that the solution retains the similarity form and that θ_c decreases monotonically from θ_∞ to θ_0.

6.2. *Case II*: $\theta_\infty > \pi/2$, $\theta_A < \pi/2$

In this case, for $\bar{t} \ll 1$ the solution takes the form of the asymptotic solution governed by (5.3) to (5.8), and illustrated in figure 8. As in all three cases, for $\bar{t} \gg 1$, the solution has the similarity form, with $\theta_c = \theta_0$. Figure 10 shows the likely qualitative form of the solution for $\bar{u}_{\pi/2} = 0.5$ and $\theta_0 = 2.27$. This has been constructed by taking the numerically calculated small-time solutions illustrated in figure 8, scaling them appropriately with $\bar{t}$, assuming that the solution retains this asymptotic form and θ_c decreases monotonically for some finite time. We then use the similarity solutions illustrated in figure 4 in a similar way for larger times. Note that oscillations on the interface are not present in the leading-order solution for small times, but do appear in the large-time solution, which suggests that they become significant at some $O(1)$ time.

6.3. *Case III*: $\theta_\infty > \pi/2$, $\theta_A > \pi/2$

In this case, for $\bar{t} \ll 1$ the contact line hangs up on the leading edge of the plate, with the asymptotic solution governed by (5.3) to (5.8), and illustrated in figure 8. As $\bar{t}$ increases, the contact angle at the fixed contact line must increase, until it exceeds the static advancing contact angle, $\theta_A > \pi/2$. The contact line can then move along the plate. We would expect this to happen when $\bar{t}$ is of $O(1)$. In terms of the dimensionless variables, the interface hangs up on the leading edge of the plate for a time proportional to $\sigma/\rho u_\infty^3$. As $\bar{t} \to \infty$, $\theta_c \to \theta_0$, and the solution takes the large-time similarity form.

If, as is physically possible, $\theta_0 = \pi$, it becomes crucial to know whether the position of the contact line in the similarity solution, $\hat{y}(0)$ remains bounded as $\theta_c \to \pi$. If it does, then the contact angle reaches π in a finite time, and the contact line moves along the plate with $\theta_c = \pi$. If not, then the contact line remains at the leading edge

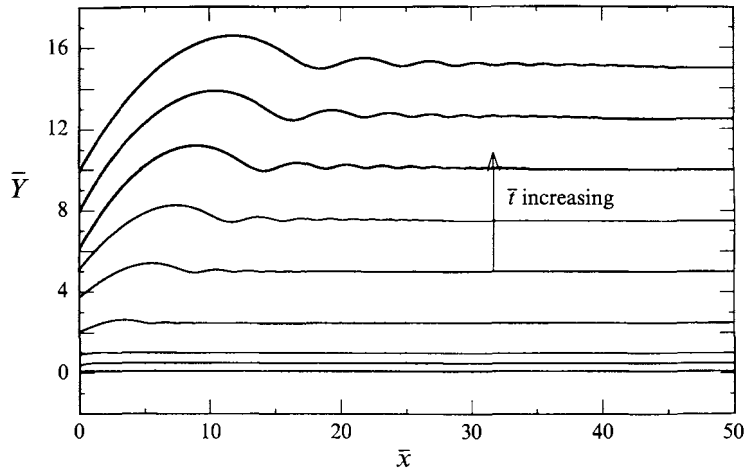

FIGURE 10. Graphs of the qualitative form of the solution for $\bar{u}_{\pi/2} = 0.5$ and $\theta_0 = 2.27$ at various times $\bar{t} = 0.1, 0.5, 1, 2.5, 5, 7.5, 10, 12.5, 15$. The first two curves use the small-time solution, the next seven use the large-time solution, five with $\theta_c = 1.67, 1.87, 2.07, 2.27$, and the last two also with $\theta_c = 2.27$. (Case II.)

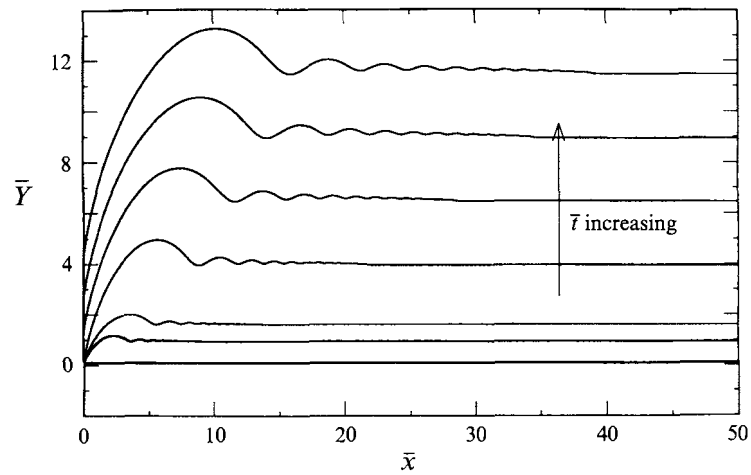

FIGURE 11. Graphs of the qualitative form of the solution for $\theta_0 = 2.87$ at various times $\bar{t}$. The contact line leaves the leading edge of the plate at around $\bar{t} = 5$. (Case III.)

of the plate, with $\theta_c \to \pi$ as $\bar{t} \to \infty$. It is worth noting however that, for the solid materials that we have so far considered for use in manufacturing local probes, the fluid/fluid/probe contact angle has never been less than 10° or greater than 170°, so, at least for the surfaces used so far, this question has not arisen.

Figure 11 shows the likely qualitative form of the solution for $\theta_0 = 2.87$. This has been constructed in a rather more *ad hoc* manner than in figures 9 and 10, by taking the numerically calculated solutions illustrated in figures 4 and 8, and scaling them with $\bar{t}$ so that the solution has the correct qualitative behaviour.

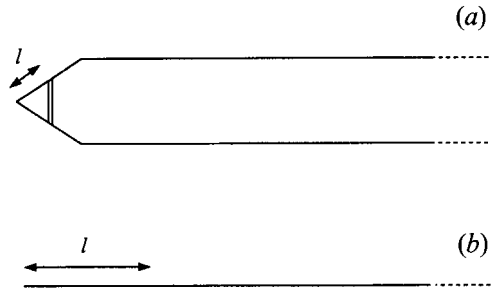

FIGURE 12. (*a*) A typical shape for a local probe, see Serizawa *et al.* 1974. (*b*) The equivalent of the length l is marked on the flat plate.

7. Implications for local probes

An essential difference between the model problem that we have studied here and the flow around a local probe is that the former has no geometrical length scale associated with it, whilst the latter certainly has. As we have seen, this means that, apart from the ratio of the fluid densities, the material properties can be scaled out of our model problem by using a length scale on which inertia balances surface tension. In order to relate this qualitatively and, in terms of orders of magnitude, quantitatively to the behaviour of fluid/fluid interfaces on the length scale of a local probe, consider a point at a distance l from the leading edge of the flat plate. This distance corresponds to that from the tip of a local probe to its sensing area. A typical probe shape is illustrated in figure 12 (see, for example, Serizawa *et al.* 1974).

In terms of the dimensionless variables defined by (3.14), $\bar{l} = \rho_A u_\infty^2 l/\sigma$. As we can see from the definition given in table 2, the dimensionless length, $\bar{l}$, is equivalent to a Weber number and indicates the strength of inertial relative to capillary forces. We have already seen in §2 (since l is of the same order of magnitude as the diameter of the probe, d) that the Weber number, *We*, is moderately small at low fluid velocities and large at high fluid velocities. In other words, at least qualitatively, at low fluid velocities $\bar{l}$ is moderately small, whilst at high velocities $\bar{l} \gg 1$. Moreover, if we want to know how much an interface has deformed when its far-field position reaches $\bar{y} = \bar{l}$, we can consider the solution of the model problem when $\bar{t} = \bar{l}$ at moderately small values of time, $\bar{t}$, or for $\bar{t} \gg 1$, respectively.

From the small-time solution that we developed in §5, we can see that the position of the moving contact line depends only on the velocity, $u_{\pi/2}$, that maintains the contact angle close to $\pi/2$. There may be no such velocity, in which case we have seen that the contact line moves rapidly along the plate with an initially singular velocity of $O(\bar{t}^{-1/3})$. If there is a velocity, $u_{\pi/2}$, that maintains the contact angle close to $\pi/2$, it can be greater than u_∞, less than u_∞, or zero, in which case the interface hangs up at the leading edge of the plate. These different possibilities are illustrated in figure 13(*a–d*). For the local probe, this suggests that the time at which the contact line passes the length l is independent of the far-field velocity of the interface. The speed of the contact line is dominated by capillary effects, as we might expect for low Weber number, *We*. Note that, although in this case the natural length scale on which surface tension balances inertia is longer than the geometrical length scale of the probe ($\bar{l}$ small), we are considering the form of the small-time solution of the model problem, in particular when the deformation of the interface is much smaller than the natural length scale. We therefore expect our conclusions to be qualitatively correct.

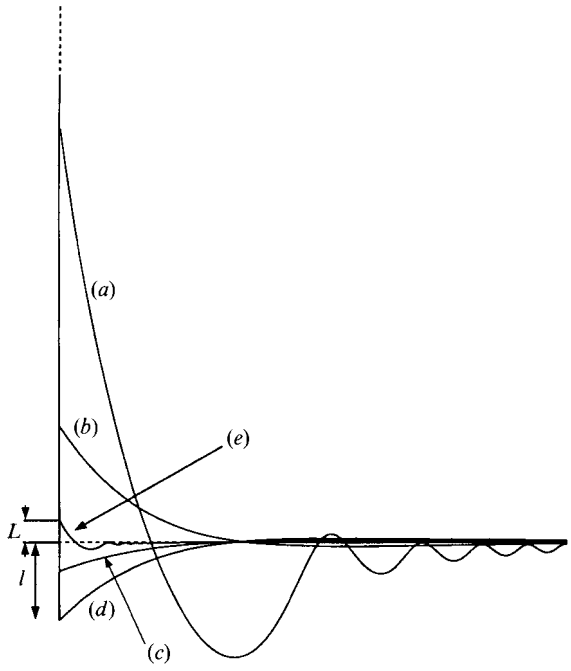

FIGURE 13. Typical shapes of the interface, firstly when $\bar{l} \ll 1$ in (*a*) case I, (*b*) case II, $\bar{u}_{\pi/2} > 1$, (*c*) case II, $\bar{u}_{\pi/2} < 1$, (*d*) case III, and secondly when $\bar{l} \gg 1$, labelled (*e*).

We studied the large-time solution of the model problem in §4. At leading order, the contact line moves at the same speed as the interface far from the plate, but leads or lags the interface, depending on whether the dynamic contact angle appropriate to this speed is less than or greater than $\pi/2$, by an amount of $O(\bar{t}^{2/3})$. When $\bar{l} \gg 1$ this means that the distance, L, by which the contact line leads or lags far-field position of the interface is only a small proportion of l, with $L/l = \bar{L}/\bar{l} = O\left(\bar{l}^{-1/3}\right)$. This is illustrated in figure 13(*e*). It is worth noting that, although *We*, and hence $\bar{l}$ can be as high as 160 for production logging applications, $160^{-1/3} \approx 0.18$ is not *very* small, so that, even at the highest velocity likely to be encountered, the contact line can lead or lag the far-field interface by as much as 20%.

8. Conclusions

In this paper we have examined large- and small-time solutions of a model problem using either Mellin transforms or a boundary integral method. Starting from the closed form of the large-time asymptotic solution, we have been able to determine the phase and amplitude of the far-field capillary waves that are generated when the contact angle is close to $\pi/2$. All of these solutions have given us insight into the factors that control the motion of a contact line over a solid surface for a range of physical parameter values relevant to the interaction of a fluid/fluid interface with a local probe.

The form of the dynamic contact angle for the two fluids and the surface of the probe, as a function of contact line velocity, is crucial in determining how an interface deforms as it meets and moves over the surface. Depending on this, the three-phase contact line may, at one extreme, hang up on the tip of the probe for some time or,

at the other extreme, move rapidly along its surface. The size of the dimensionless Weber number, which measures the relative strength of inertial and capillary forces, also affects the size of the deformation.

We would like to thank Anthony Pearson for the encouragement that he has given us.

Appendix. The solution of the linearized problem as $\xi \to \infty$

Here we are concerned with finding the asymptotic behaviour of (4.46),

$$\tilde{y}(\xi) = -\frac{2}{9}\left(\frac{27}{4(1+\rho)}\right)^{1/3}\frac{\Gamma\left(\frac{1}{2}\right)}{\Gamma\left(\frac{1}{3}\right)\Gamma\left(\frac{2}{3}\right)}\frac{1}{2\pi\mathrm{i}}\int_{c-\mathrm{i}\infty}^{c+\mathrm{i}\infty}\frac{\Gamma\left(\frac{1}{3}p+\frac{2}{3}\right)\Gamma\left(\frac{1}{3}p\right)\cos(\frac{1}{2}\pi p)R^{-p/3}}{\Gamma\left(\frac{1}{3}p+\frac{5}{6}\right)(1+p)\sin(\frac{1}{3}\pi(p+1))}\mathrm{d}p, \tag{A 1}$$

in the limit $\xi \to \infty$, where $R = 4(1+\rho)\xi^3/27$ and $0 < c < 2$. This will tell us how the interface deforms far from the contact line. Some elementary manipulations of the trigonometric functions show that

$$\tilde{y}(\xi) = \frac{\pi^{1/2}\xi}{9\Gamma\left(\frac{1}{3}\right)\Gamma\left(\frac{2}{3}\right)}(K - 4J), \tag{A 2}$$

where

$$J = \frac{1}{2\pi\mathrm{i}}\int_{d-\mathrm{i}\infty}^{d+\mathrm{i}\infty}\frac{\Gamma\left(s-\frac{1}{3}\right)\Gamma\left(s+\frac{1}{3}\right)\cos(\frac{1}{2}\pi s)}{\Gamma\left(s+\frac{1}{2}\right)s}R^{-s}\mathrm{d}s, \tag{A 3}$$

$$K = \frac{1}{2\pi\mathrm{i}}\int_{d-\mathrm{i}\infty}^{d+\mathrm{i}\infty}\frac{\Gamma\left(s-\frac{1}{3}\right)\Gamma\left(s+\frac{1}{3}\right)}{\Gamma\left(s+\frac{1}{2}\right)s\cos(\frac{1}{2}\pi s)}R^{-s}\mathrm{d}s, \tag{A 4}$$

and $1/3 < d < 1$. In order to determine the asymptotic behaviour of K as $R \to \infty$, we note that the factor of $1/\cos\left(\frac{1}{2}\pi s\right)$ means that the integrand in (A 4) decays more rapidly than the integrand in (A 1). This allows us to close the contour of integration to the right of the pole at $s = 1$, and, on applying the residue theorem, show that

$$K \sim \frac{4\Gamma\left(\frac{1}{3}\right)\Gamma\left(\frac{2}{3}\right)}{3\pi^{3/2}R}, \quad \text{as } R \to \infty. \tag{A 5}$$

We now turn our attention to J, and firstly note that

$$\frac{\mathrm{d}J}{\mathrm{d}R} = -\frac{1}{2R}(J_- + J_+), \tag{A 6}$$

where

$$J_\pm = \frac{(\pm\mathrm{i}R)^{-d}}{2\pi\mathrm{i}}\int_{-\mathrm{i}\infty}^{+\mathrm{i}\infty}\frac{\Gamma\left(d-q-\frac{1}{3}\right)\Gamma\left(d-q+\frac{1}{3}\right)}{\Gamma\left(d-q+\frac{1}{2}\right)}(\pm\mathrm{i}R)^q\,\mathrm{d}q. \tag{A 7}$$

Now, by using results given by Gradshteyn & Ryzhik (1980, p. 659, equation 17 and p. 1062, equation 9.235.1), we find that

$$J_\pm = \frac{\mathrm{e}^{\mp\mathrm{i}R/2}}{\pi^{1/2}}K_{-1/3}\left(\pm\tfrac{1}{2}\mathrm{i}R\right). \tag{A 8}$$

On substituting this back into (A 6), and using the fact that $K_{-1/3}(z) \sim \mathrm{e}^{-z}(\pi/2z)^{1/2}$ as $z \to \infty$, we find that $\mathrm{d}J/\mathrm{d}R \sim -\cos\left(R+\pi/4\right)/R^{3/2}$ as $R \to \infty$, and hence that

$$J \sim -\frac{\sin\left(R+\frac{1}{4}\pi\right)}{R^{3/2}}, \quad \text{as } R \to \infty. \tag{A 9}$$

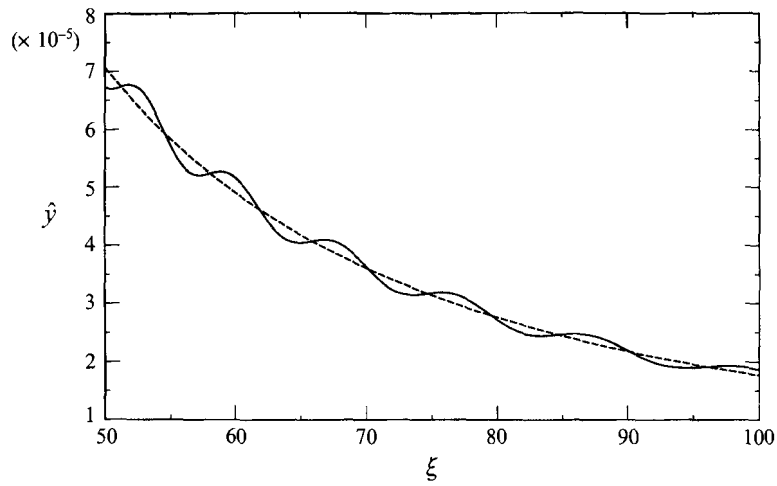

FIGURE 14. The behaviour of $\hat{y}(\xi)$ as $\xi \to \infty$, for $\rho = 0.8$. The numerical evaluation of (A 1) is the solid line, whilst the dashed line is $\hat{y} = 1/\pi(1+\rho)\xi^2$.

We can now substitute (A 5) and (A 9) into (A 2), and arrive at

$$\hat{y}(\xi) \sim \frac{1}{\pi(1+\rho)\xi^2} + \frac{4\pi^{1/2}}{9\Gamma\left(\frac{1}{3}\right)\Gamma\left(\frac{2}{3}\right)}\left\{\frac{27}{4(1+\rho)}\right\}^{3/2}\frac{\sin\left(4(1+\rho)\xi^3/27+\pi/4\right)}{\xi^{7/2}},$$

as $\xi \to \infty$. (A 10)

The position of the interface decays to the far-field position as ξ^{-2}, whilst the amplitude of the waves on the interface decays more rapidly, as $\xi^{-7/2}$, with a wavelength that decays as ξ^{-2}. Equation (A 10) has the same functional form as that obtained by Keller & Miksis (1983) for the free surface case, $\rho = 0$.

As discussed in §4.1, the integral in (A 1) can be evaluated numerically, and is illustrated for a particular case, $\rho = 0.8$, in figure 14, along with the leading-order asymptotic behaviour calculated above, $\hat{y} \sim 1/\pi(1+\rho)\xi^2$. These are in good agreement, although the oscillations shown in figure 14 are a numerical artifact. The more rapid oscillations in the far-field solution could, in principle, be resolved by a far more accurate numerical evaluation of the integral. We have not attempted this here, since the fine-scale oscillatory features of the solution are very hard to resolve numerically. The asymptotic expression (A 10) is clearly the most appropriate way to describe the solution for $\xi \gg 1$.

REFERENCES

COX, R. G. 1986 The dynamics of the spreading of liquids on a solid surface. Part 1. Viscous flow. *J. Fluid Mech.* **168**, 169–194.

DUSSAN V., E. B. 1976 The moving contact line: the slip boundary condition. *J. Fluid. Mech.* **77**, 665–684.

DUSSAN V., E. B. 1979 On the spreading of liquids on solid surfaces: Static and dynamic contact lines. *Ann. Rev. Fluid Mech.* 77, 371–400.

GRADSHTEYN, I. S. & RYZHIK, I. M. 1980 *Tables of Integrals, Series, and Products*, Corrected and Enlarged Edition. Academic Press.

JEFFREYS, H. & JEFFREYS, B. S. 1962 *Methods of Mathematical Physics*. Cambridge University Press.

KELLER, J. B. & MIKSIS, M. K. 1983 Surface tension driven flows. *SIAM J. Appl. Maths* **43**, 268–277.

KING A. C. 1991 Moving contact lines in slender fluid wedges. *Q. J. Mech. Appl. Maths* **44**, 173–192.

KING, L. V. 1914 Convection of heat from small cylinders in a stream of fluid. *Proc. R. Soc. Lond.* A **214**, 373–432.

MOUJAES, S. *1990* Testing of a spherical dual-tipped optical fibre probe for local measurements of void fraction and gas velocity in two-phase flows. *Can. J. Chem. Engng* **68**, 504–510.

PRESS, W. H., TEUKOLSKY, S. A., VETTERLING, W. T. & FLANNERY, B. P. 1986 *Numerical Recipes.* Cambridge University Press.

SEKOGUCHI, K., TAKEISHI, M., NISHIURA, T., KANO, H. & NOMURA, T. 1985 Multiple optical fiber probe technique for measuring profiles of gas-liquid interface and its velocity. In *Proc. Winter Annual Meeting of the ASME*, FED Vol. 23.

SERIZAWA, A., KATAOKA, I. & MICHIYOSHI, I. 1974 Turbulence structure of air-water bubbly flow. *Intl J. Multiphase Flow* **2**, 221–259.